

# Buoyancy-driven flow between two rooms coupled by two openings at different levels

L. P. THOMAS<sup>1</sup>, B. M. MARINO<sup>1</sup>,  
R. TOVAR<sup>2</sup> AND P. F. LINDEN<sup>3</sup>

<sup>1</sup>Instituto de Física Arroyo Seco, Facultad de Ciencias Exactas, Universidad Nacional del Centro de la Pcia. de Buenos Aires, Pinto 399, B7000GHG Tandil, Argentina

<sup>2</sup>Centro de Investigación en Energía UNAM, Apdo. Postal 34, Temixco Mor. 62580 México

<sup>3</sup>Department of Mechanical and Aerospace Engineering, University of California, San Diego, 9500 Gilman Drive, La Jolla, CA 92093-0411, USA

(Received 27 October 2006 and in revised form 7 September 2007)

The stack-driven flow between two interconnected rooms produced by a single heat source is studied. In particular, the features of the transient flow for different positions and areas of two openings in the shared vertical wall are analysed. An analytical model provides the time evolution of the stratified flows in rooms of any size. The concept of an *equivalent* layer representing a non-uniform density profile, which is useful in other contexts, is included in the theoretical approach and provides physical insight and aids the mathematical solution of the problem. New salt-bath experiments are performed to simulate the thermal forcing between the rooms, to validate the model and to analyse the mixing generated and the effects of a source of volume in the configuration studied.

---

## 1. Introduction

Sources of buoyancy, such as occupants or equipment, may generate significant flows in buildings. These sources tend to be isolated and produce buoyant plumes that rise above them. The warm air accumulates near the ceiling and a stable stratification is established within each room of the building. Different vertical stratifications generated in adjacent rooms with different heat loads can drive flows through openings in the dividing walls. Thus the ventilation patterns and the temperature distributions in the whole building depend on the geometry of these interconnections and the distribution of the heat loads in the rooms. For example, the pressure difference caused by a temperature difference of 3 °C between two rooms of height 2 m will drive a flow of about 0.6 m s<sup>-1</sup>, which is strong enough to transport heat and pollutants rapidly from one room to another. However, if only the upper part of a room is warm, there will be no flow unless there is an opening in this upper region.

Lin & Linden (2002) examined the time-dependent flow and stratification between two rooms with interconnecting openings located at the top and bottom of a dividing wall. The heights of the rooms were the same but the floor areas differed, and heating was applied only in the smaller room. As this room was heated, warm air flowed out through the top opening into the larger cold room, and travelled across the ceiling. This outflow was matched by an inflow of cold air through the lower opening. The flow in the heated room is that of displacement ventilation, with cool air entering at low levels and warm air leaving at high levels (Linden 1999). If the larger room

is infinite in size, this situation is equivalent to natural displacement ventilation of a single room connected to the exterior and a steady state develops with a two-layer stratification in the smaller room. The height of the interface depends only on the size of the openings and the height of the room, and is determined by equating the volume flux in the plume with that through the openings (Linden, Lane-Serff & Smeed 1990).

In a finite-size room, once the warm air reaches the far wall of the unheated room it begins to accumulate in an upper layer of increasing depth. Consequently, the pressure difference across the upper opening decreases and the outflow decreases accordingly. Since the interface height is determined by this volume flux and the plume volume flux increases with height, the interface descends. Furthermore, since the temperature in the plume decreases with height, this lowering of the interface means that the upper layer in the heated room increases in temperature with time. Thus warmer air subsequently enters the unheated room producing stable stratification there. The temporal behaviour in the heated room is determined by a time scale related to the size of the unheated room.

In this paper, we extend that work by considering interconnections at other heights in the dividing wall and a connection to the exterior through an exit opening at the bottom of the unheated space. Since the exterior is colder than the air within the spaces, no flow will occur through this opening unless there is a source of volume as well as a source of buoyancy. This can be thought of as an example of an air-conditioned space where cold air is introduced through the ceiling and removed in a return duct also in the ceiling – the geometry is then inverted from the previous discussion.

We develop a theoretical model that describes the temporal evolution of the flow for such a situation in §2. The introduction of an *equivalent height*, as proposed by Marino, Thomas & Linden (2005), gives extra physical insight into the analytical approach. The model is tested against laboratory experiments which incorporate mixing and volume supply of the source. The experimental results are presented, compared with the theoretical findings and discussed in §3. Our conclusions are presented in §4.

## 2. Theoretical model

### 2.1. Initial filling of the forced room

Consider two rooms of height  $H$  and horizontal areas  $S_f$  and  $S_u$  (figure 1). The spaces are connected to each other by means of openings 1 and 2 located at heights  $h_1$  and  $h_2$  from the floor, respectively, with  $h_2 < h_1 < H$ . In the space we distinguish the ‘forced’ room, there is a turbulent plume rising from a source of buoyancy located at the floor. The other space is called the ‘unforced’ room. Both spaces initially contain air of density  $\rho$ .

The air heated by the buoyancy source forms a plume that reaches the ceiling and spreads sideways covering the entire top surface  $S_f$  of the forced room, forming a warm upper layer. As the plume rises, it entrains air from its surroundings and carries it into the upper layer, which increases in depth with time. There is no exchange of warm air between the two rooms provided the interface does not reach opening 1 and, as assumed throughout, the plume width is less than that of the forced room.

Initially we restrict our attention to the case where the plume is a ‘pure’ plume with constant buoyancy flux but with zero volume and momentum fluxes at the source. Thus without the addition of volume, there is no flow to the exterior and so, as mentioned above, we can consider the enclosures as being closed to the exterior

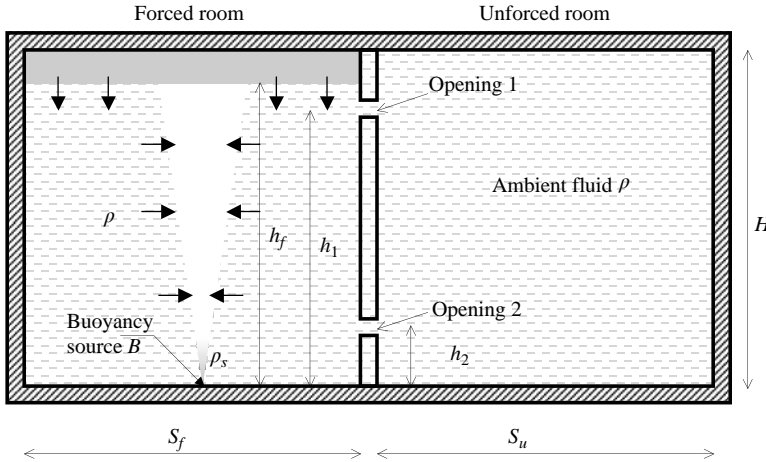


FIGURE 1. Sketch of the situation modelled when the forced room is beginning to fill.

environment. In this case, the classical ‘filling box’ model developed by Baines & Turner (1969), which we now briefly summarize, describes the flow.

The volume  $Q_p$  flux and the reduced gravity  $g' = g\Delta\rho/\rho$  of a Boussinesq turbulent plume at a height  $h$  above the source are related to the buoyancy flux  $B$  by

$$B = g' Q_p, \tag{2.1}$$

$$Q_p = C(Bh^5)^{1/3}, \tag{2.2}$$

$$g' = \frac{1}{C}(B^2h^{-5})^{1/3}, \tag{2.3}$$

where  $C$  ( $\approx 0.09$ ) is a dimensionless constant related to an empirically determined entrainment coefficient  $\alpha$ ; for example  $C = (6/5)\alpha(9\alpha/10)^{1/3}\pi$  for ‘top hat’ profiles (Morton, Taylor & Turner 1956; Turner 1986).

Baines & Turner (1969) studied the evolution of the interface or ‘first front’ of buoyant fluid as it descends from the ceiling. Since all the fluid added to the layer above the front comes from the lower ambient fluid as a result of the entrainment into the plume, the front evolution is given by a local balance of volume at the interface  $h = h_f$ , in the form

$$S_f \frac{dh_f}{dt} = -Q_p(h_f). \tag{2.4}$$

Substituting (2.2) into (2.4) and solving the differential equation, it follows that

$$\xi_f = \left(1 + \frac{2C}{3}\tau\right)^{-3/2}, \tag{2.5}$$

with  $\xi_f = h_f/H$  and  $\tau = t/(S_f B^{-1/3} H^{-2/3})$ . Thus the dimensionless time  $\tau_1$  taken for the interface to reach opening 1 located at  $\xi_1 = h_1/H$  is

$$\tau_1 = \frac{3 [(\xi_1)^{-2/3} - 1]}{2C}. \tag{2.6}$$

Hence  $\tau_1$  depends on the height of the top opening and the plume features, but it is independent of the reduced gravity distribution in the warm layer.

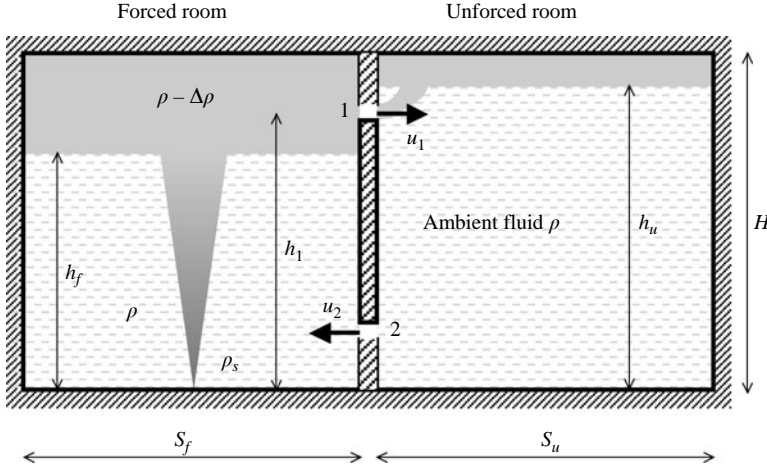


FIGURE 2. Sketch of the situation modelled when mixed fluid starts to flow to the unforced room.

Baines & Turner (1969) and Worster & Huppert (1983) used approximations to obtain the density profile of the warm layer. The actual profile is an intermediate between two extreme cases – no mixing and complete mixing inside the buoyant layer.

If there is no mixing, the density profile above the first front is given by (2.3), and the total buoyancy in the warm layer is

$$\int_{h_f}^H S_f g' dz = \frac{3}{2C} \frac{S_f B^{2/3}}{H^{2/3}} (\xi_f^{-2/3} - 1), \tag{2.7}$$

which is equal to  $Bt$  if  $\xi_f(\tau)$  is given by (2.5). Thus we check that the total buoyancy in the warm layer is a linear function of time, as expected when a constant-flux source is considered.

In the case of complete mixing, the uniform but time-dependent reduced gravity  $g'_f(t)$  in the warm layer satisfies

$$S_f g'_f (H - h_f) = \int_{h_f}^H S_f g' dz. \tag{2.8}$$

In such a case, the evolution of the system may also be given by the conservation of the total buoyancy in the warm layer as

$$\frac{d[S_f g'_f (H - h_f)]}{dt} = B, \tag{2.9}$$

instead of imposing the volume conservation (2.4). As a result, the advance of the front is again (2.5), but now calculated using the uniform reduced gravity  $g'_f(t) \neq g'(t)$ .

### 2.2. Venting the forced room

After time  $\tau_1$ , the warm fluid flows through opening 1 into the unforced room while the ambient fluid flows in the opposite direction through opening 2 (figure 2). For  $\xi_1 < \xi_u < 1$ , the warm fluid moves upwards to the ceiling of the unforced room where it accumulates, while the forced room incorporates ambient fluid from the unforced room.

In the forced room, the situation is described by the ‘emptying filling box’ model proposed by Linden *et al.* (1990). The volume fluxes through the top and bottom

openings are given by

$$Q_1 = A_1^* u_1, Q_2 = A_2^* u_2, \quad (2.10)$$

where  $u_1, u_2$  are the mean velocities and  $A_1^*, A_2^*$  are the ‘effective areas’ of the top and bottom openings, respectively. The corresponding discharge coefficients accounting for streamline contraction are included in the values of  $A_1^*$  and  $A_2^*$ . Thus the values of  $A_i^*$  ( $i = 1, 2$ ) range from 0.6 (sharp orifice) to 0.98 (streamline shapes) times the geometrical areas of the openings, depending on the opening shape and profile. The discharge coefficient of a planar slit as used in the experiments described in §3, ranges from 0.611 (potential flow) to 0.687 (high Reynolds number see e.g. Ali & Foss 2003).

When the volume of fluid supplied by the source is negligible, volume conservation implies

$$Q_1 = Q_2 = Q. \quad (2.11)$$

Adapting the result obtained by Linden *et al.* (1990) to the present case with  $h_1 \neq H$ ,

$$Q = A^* \sqrt{g'_f (h_1 - h_f)}, \quad (2.12)$$

where  $g'_f = g'_f(t)$  is the average reduced gravity in the forced room and

$$A^* = \frac{A_1^* A_2^*}{\sqrt{\frac{1}{2} (A_1^{*2} + A_2^{*2})}} \quad (2.13)$$

is the effective area of the openings.

Because  $g'_f$  varies with time, the interface height in the forced room is given by the buoyancy conservation

$$\frac{d[S_f g'_f (H - h_f)]}{dt} = B - g'_f Q. \quad (2.14)$$

Note that (2.14) is different from the volume conservation used by Lin & Linden (2002) that in the present notation reads

$$S_f \frac{dh_f}{dt} = -Q_p(h_f) + Q. \quad (2.15)$$

As an approximation for  $g'_f$ , we use

$$g'_f = \theta g', \quad (2.16)$$

where  $g'$  is given by (2.3) and  $\theta$  is a constant of the order of unity. Substitution of (2.12) and (2.16) into (2.14) leads to

$$\frac{d\xi_f}{d\tau} = \frac{A^*}{H^2} \frac{\sqrt{\frac{\theta}{C} \xi_f^{-5/3} (\xi_1 - \xi_f) - \frac{C}{\theta} \xi_f^{5/3}}}{\frac{5}{3} \xi_f^{-1} - \frac{2}{3}}, \quad (2.17)$$

with  $\xi_1 = h_1/H$ .

Since the finite size of the unforced room does not affect the flow at this stage (see § 2.3), the time scale is the same as that in the previous stage ( $S_f B^{-1/3} H^{-2/3}$ ). The evolution of  $\xi_f$  depends on the entrainment constant  $C$  modified by the mixing in the warm layer by means of  $\theta$ , and the dimensionless geometrical parameters, namely, the height  $\xi_1$  of the top opening and the vent area  $A^*/H^2$ .

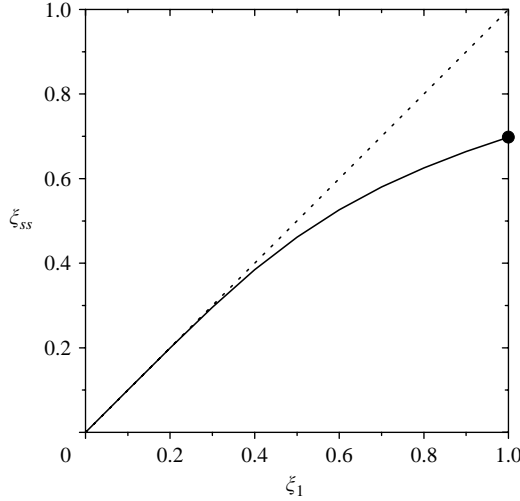


FIGURE 3. Position of the interface in the forced room during the steady-state regime (solid line) and  $\xi_{ss} = \xi_1$  (dotted line). The point at  $\xi_1 = 1$  corresponds to the result obtained by Linden *et al.* (1990).

The flow in the forced room tends towards a steady state. Putting  $d\xi_f/d\tau = 0$  in (2.17), the position  $\xi_{ss}$  of the interface is given by

$$\frac{A^*}{H^2} = C^{3/2} \left( \frac{\xi_{ss}^5}{(\xi_1 - \xi_{ss})} \right)^{1/2}, \tag{2.18}$$

for  $\theta \approx 1$ . This equation is a more general relationship than that obtained by Linden *et al.* (1990) for the particular case with  $h_1 = H$  (their equation 2.11a). Figure 3 shows the position  $\xi_{ss}$  calculated using (2.18) as a function of  $\xi_1$  which shows that the distance between the vent and the steady-state front position is reduced significantly when  $\xi_1$  decreases; in particular  $\xi_{ss} \approx \xi_1$  for  $\xi_1 \lesssim 0.4$ .

During the transient flow, warmer fluid flows into the unforced room and forms a stable stratification. The hydrostatic pressure in the unforced room is obtained by integration of the vertical density profile  $\rho_u(z)$  inside the warm layer. In order to simplify the solution, an equivalent height  $h_u$  is defined for which a warm layer with uniform density  $g'_f(t)$  – the density of the forced room – generates the same pressure difference in the unforced room, that is

$$h_u g'_f = g \int_0^H \frac{(\rho - \rho_u)}{\rho_u} dz. \tag{2.19}$$

Therefore, the buoyancy excess is

$$m_f = g'_f S_f (H - h_f) \quad \text{in the forced room,} \tag{2.20a}$$

$$m_u = g'_f S_u (H - h_u) \quad \text{in the unforced room.} \tag{2.20b}$$

Normally  $h_u$  does not coincide with the actual height  $h_u^*$  of the interface defined by the maximum density gradient in the warm layer. Later, we will return to the stratification of the unforced room.

Conservation of mass implies

$$S_f g'_f (H - h_f) + S_u g'_f (H - h_u) = Bt, \tag{2.21}$$

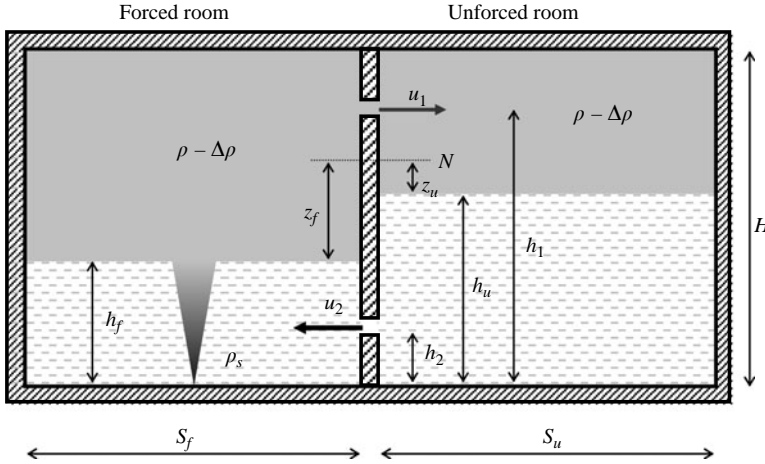


FIGURE 4. Sketch of the situation modelled when the mixed fluid in the unforced room has exceeded opening 1.

where  $g'_f$  is given by (2.16) for  $\tau > \tau_1$ . Note that (2.21) is also different from the volume conservation relationship

$$S_u \frac{dh_u}{dt} = -Q, \tag{2.22}$$

used by Lin & Linden (2002) for calculating  $h_u$ . Substituting (2.16) into (2.21), it follows that  $\xi_u = h_u/H$  is

$$\xi_u = 1 - R \left[ \frac{C}{\theta} \xi_f^{5/3} \tau - (1 - \xi_f) \right], \tag{2.23}$$

where  $\tau = t/(S_f B^{-1/3} H^{-2/3})$  as before and  $R = S_f/S_u$  is the aspect ratio of the areas of the rooms.

This stage continues until the front in the unforced room reaches opening 1. The time  $\tau_2$  at which this occurs depends on the solution of the system formed by (2.17) and (2.23) which involve the parameters of the problem:  $C/\theta$ ,  $A^*/H^2$ ,  $\xi_1$ , and  $R$ .

### 2.3. Coupling the flows in both rooms

For  $\xi_1 > \xi_u > \xi_2$ , the state in the unforced room affects the flow in the forced room (figure 4). At some level  $h_N$ , the neutral level, the hydrostatic pressure in both rooms is the same and this height determines the direction of the flow through the openings. The fluid flows from the forced to the unforced room through an opening above this level, and in the opposite direction below.

We now introduce  $z_f$  and  $z_u$  as the vertical distances between the neutral level and the heights  $h_f$  and  $h_u$  in the forced and unforced rooms, respectively. Using Bernoulli's theorem, the velocities of the fluid through the openings are

$$u_1^2 = 2g'_f(h_1 - h_f - z_f) - 2g'_f(h_1 - h_u - z_u), \tag{2.24}$$

$$u_2^2 = 2g'_f z_f - 2g'_f z_u, \tag{2.25}$$

for  $h_2 \leq (h_u, h_f) \leq h_1$ .

By eliminating  $h_1$  from (2.24) and defining  $z = z_f - z_u$ , (2.24) and (2.25) become

$$u_1^2 = 2g'_f[(h_u - h_f) - z], \tag{2.26}$$

$$u_2^2 = 2g'_f z. \tag{2.27}$$

At this stage, the flow is independent of the height of both openings and the neutral level, and depends on the differences  $(h_u - h_f)$  and  $(z_f - z_u)$ . Note also  $z_f$  and  $z_u$  can be positive or negative, and then (2.26)–(2.27) can represent the situations in which  $h_f$  and  $h_u$  are greater or less than  $h_N$ .

Equations (2.26) and (2.27) are the relationships that describe the ventilation of one room through two openings to an infinite environment according to the model developed by Linden *et al.* (1990) (their equations 2.2a and 2.2b, respectively) with a proper definition of distances from the fronts to the neutral level and to the floor. Thus the problem of the flow inside two interconnected rooms is reduced to the problem of an equivalent single room ventilated to the environment.

Using the whole volume conservation (2.11), it follows that

$$Q = A^* \sqrt{g'_f (h_u - h_f)}, \quad (2.28)$$

where  $A^*$  is given by (2.13). The evolutions of the interfaces in the forced and unforced rooms are given by (2.14) and (2.23), respectively. Substituting  $\xi_1$  by  $\xi_u$  in (2.17), the dimensionless equations for the flow in the two connected rooms are obtained:

$$\frac{d\xi_f}{d\tau} = \frac{\frac{A^*}{H^2} \sqrt{\frac{\theta}{C} \xi_f^{-5/3} (\xi_u - \xi_f)} - \frac{C}{\theta} \xi_f^{5/3}}{\frac{5}{3} \xi_f^{-1} - \frac{2}{3}} \quad (2.29)$$

and (2.23), which constitute a system of two coupled ordinary differential equations that can be easily integrated numerically. The initial condition for the integration is taken from the values of the variables obtained at the end of the stage described in § 2.2.

Comparing the two terms of the numerator on the right-hand side of (2.29), we find that the flux between the two rooms is important when

$$\frac{A^*}{H^2} > \left(\frac{C}{\theta}\right)^{3/2} \approx 0.03. \quad (2.30)$$

The flow in the forced room evolves as in a closed room if  $A^*/H^2 \ll (C/\theta)^{3/2}$  and then the front position may be approximated by (2.5). On the contrary, the buoyancy supplied by the source in the forced room is strongly ventilated to the unforced room for  $A^*/H^2 \gg (C/\theta)^{3/2}$ . In such a situation, the aspect ratio  $R$  affects the evolution of the flow in both rooms.

#### 2.4. Solutions

Figure 5 shows the comparison between the present analytical results and those obtained by Lin & Linden (2002) for the special case studied there in which openings 1 and 2 are at the top and bottom of the shared wall, respectively ( $\xi_1 = 1$ ,  $\xi_2 = 0$ ). As expected, the positions of both fronts given by the present model tend to be the same for long times. The evolution of the front in the forced room is near to that predicted by Lin & Linden (2002) (dashed line) even though volume conservation (see (2.15)) was used by them. However, the evolution of the position of the equivalent front in the unforced room shows a quite different behaviour. This may be a result of the use of volume conservation (2.19) instead of the buoyancy conservation employed here for calculating the progress of this interface.



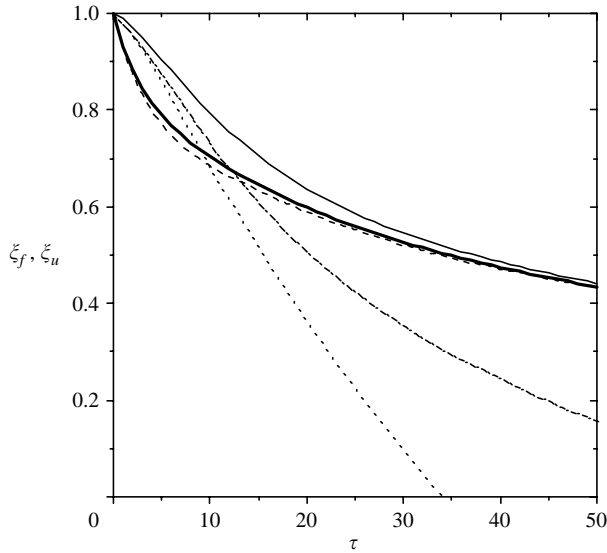


FIGURE 5. Evolutions of the dimensionless front positions in the forced (thick solid line) and unforced (thin solid line) rooms for the case of two equal size rooms. The dashed, dash-dotted and dotted lines correspond to  $\xi_f$ ,  $\xi_u$  and  $h_u^*/H$ , respectively, calculated using the model introduced by Lin & Linden (2002). ( $\xi_1 = 1$ ;  $A^*/H^2 = 0.02$ ;  $R = 1$ .)

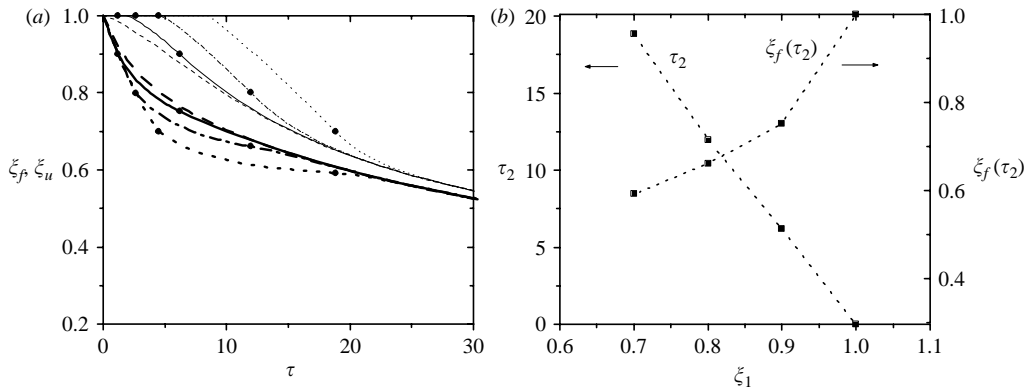


FIGURE 6. (a) Evolutions of the dimensionless front positions for  $\xi_f, \xi_u > \xi_2$  in the forced (thick lines) and unforced (thin lines) rooms:  $\xi_1 = 1, \xi_2 = 0$  (dashed line);  $\xi_1 = 0.9, \xi_2 = 0.1$  (solid line);  $\xi_1 = 0.8, \xi_2 = 0.2$  (dash-dotted line);  $\xi_1 = 0.7, \xi_2 = 0.3$  (dotted line). The front positions at  $\tau_1$  and  $\tau_2$  are indicated by circles. (b) Values of time  $\tau_2$  and position  $\xi_f(\tau_2)$  obtained for the same cases in (a). ( $R = 1$ ;  $A^*/H^2 = 0.02$ ).

Figure 6(a) shows the dimensionless positions of the interfaces as a function of time for different heights of the top and bottom openings. For  $\xi_1 < 1$ , the front in the forced room evolves as that in a closed room during the initial stage as explained in §2.1. In the unforced room the front is formed after a time  $\tau_1$  and then begins to move down as described in §2.2; after a time  $\tau_2$ , the solution given in §2.3 is applied. Figure 6(b) shows  $\tau_2$  and the height of the interface in the forced room at this time,

Run	Opening 1		Opening 2		$t_s$ (s)
	$\xi_1$	$A/H^2$	$\xi_2$	$A/H^2$	
1	1	0.042	0	0.042	460
2	1	0.023	0	0.023	705
3	1	0.042	0.36	0.042	2190
4	1	0.042	0.70	0.042	3780
5	0.75	0.042	0	0.042	520
6	0.33	0.042	0	0.042	870
7	0.66	0.042	0.36	0.042	1420
8	1	0.005	0.91	0.005	6800
9	0.75	0.023	0	0.023	620

TABLE 1. Values of the main parameters varied in the experiments. The time  $t_s$ , at which mixed fluid starts to pass through the exit holes, is also included.

$\xi_f(\tau_2)$ , obtained in the present cases;  $\xi_f(\tau_2)$  and  $\xi_u(\tau_2)$  are also marked with solid circles on the curves of figure 6(a).

A lower position of opening 1 delays the beginning of the exchange between both rooms because of the increase of  $t_1$ . However, the lower  $\xi_1$ , the larger  $\tau_2$ , and larger changes are seen in the evolution of the fronts at the beginning of the unforced room filling. This stage lasts longer than ten characteristic times, and increases with a reduction of the height of opening 1. For  $t > \tau_2$ , the evolution of the dimensionless front positions in both rooms tends to be the same in all cases because the stronger flow generated between the rooms compensates for the initial differences.

The solutions for different dimensionless opening areas  $A^*/H^2$  show an effect upon the flow according to the condition (2.30). For  $A^*/H^2 = 0.1 > 0.03 \approx (C/\theta)^{3/2}$ , both fronts tends to evolve closely to each other after  $\tau_1$ , so that the system behaves as a single room. For smaller  $A^*/H^2$ , the front in the forced room evolves quicker than that in the unforced room. Thus for  $A^*/H^2 = 0.03 \approx (C/\theta)^{3/2}$ , the evolutions of the fronts are slightly separated, and the difference between the fronts heights increases as the value of  $A^*/H^2$  diminishes, in such a way that for  $A^*/H^2 = 0.003$ , the flow in the forced room initially behaves similarly to that in a closed room.

### 3. Experimental results and comparisons with the theory

#### 3.1. Experimental set-up

The physical model consisted of a Perspex box 0.248 m high, 0.60 m long and 0.20 m wide (interior size) with an inner wall in the middle of the box forming two spaces each of 0.295 m long. The dividing vertical wall contained two rectangular openings at different levels as given in table 1.

The box was initially filled with tap water ( $\rho = 0.998 \text{ g cm}^{-3}$ ), and a nozzle especially designed to produce a lazy turbulent plume (Hunt & Kaye 2001) simulated the source of buoyancy. The nozzle, fixed at the top of the forced room, released salt water ( $\rho_s = 1.034 \text{ g cm}^{-3}$ ) at a constant flow rate  $Q_s = 2.57 \text{ cm}^3 \text{ s}^{-1}$  in all the experiments. The density of the salt water and the flow rate were measured using an Anton Paar DMA 5500 density meter and an in-line water flow meter, respectively. The buoyancy flux was  $B = g Q_s (\rho_s - \rho_w) / \rho_w = 90.9 \text{ cm}^4 \text{ s}^{-3}$ . Holes of diameter 0.0342 and 0.0415 m drilled in the ceiling of the unforced room provide an exit of the input fluid. The fluid released from these holes was collected to check the buoyancy flux  $B$  by measuring its volume and mass at the end of each experiment.

Since salt water is used to model the buoyant fluid, the experimental set-up is vertically inverted with respect to the arrangement shown in figures 1, 2 and 4 (for details see Linden 1999; Lin & Linden 2002). However, hereinafter the experimental findings are introduced according to the configuration and nomenclature given in §2.

The nozzle acts as a source of fluid that may change the neutral level in which the hydrostatic pressure is the same in both rooms (see §2.3). The height difference between the position of the interface in the forced room and that in the unforced room associated to this effect may be estimated by using the experimental value of  $Q_s$  instead of  $Q$  in (2.28). We find that the difference in height is 0.02 cm when the smallest openings are used (Run 8), which is negligible compared with the measured heights.

A panel of fluorescent lights and a diffusive screen were located behind the model and a video camera was placed 5.2 m on the other side. The dye added to the salt water reduces the intensity of the light passing through the model and the intensity reduction is related to the fluid density averaged along the light path. The width-average density distribution is obtained by processing the images taken by the video camera with the method applied by Cenedese & Dalziel (1998).

The images are digitized and processed with *DigImage* software (Dalziel 1993, 1995). The average of the horizontal intensities in each pixel row in carefully chosen windows without obstructions are calculated. These average intensity values as a function of the vertical position give the density profile as a function of height. As the vertical stratification is formed a short time after the beginning of the experiment, the integration of the vertical density profile provides an estimate of the mass in each room. As seen later, the total mass excess (that is, the buoyancy excess defined in theory) in both rooms initially follows a linear function of time because the net buoyancy flux input remains constant until mixed water starts to escape through the exit holes in the unforced room. This behaviour allows us to estimate the density obtained by image processing with an error less than 2%. An additional check of this value comes from the measurement of the volume and weight of the total fluid performed at the end of each experiment. The uncertainty of the height values is about the size of a pixel in the images, that is, less than 0.05% of the box height.

### 3.2. Effects of the opening size

As described in §2, the flow between the rooms has to be described by means of a balance between the buoyancy integrated in each chamber. Therefore, volumes (determined by front positions) and density distributions are not important separately but together, and therefore the comparisons should be done mainly on these integrated buoyancy values.

Figure 7 shows a comparison between the measurements of the buoyancy excess in both chambers for Runs 1 (squares), 2 (circles) and 8 (triangles) and the corresponding theoretical predictions. There is a good agreement for  $t \lesssim t_s$  as expected. The relative error between theory and experimental results at  $\tau \approx 30$ , for example, is less than 6%, except for the unforced chamber in Run 8 where the value of the buoyancy excess is very small. For  $t > t_s$ , the agreement for the total buoyancy excess is gradually lost because the total buoyancy conservation (2.21) is no longer valid owing to the fluid loss from the box. However, the theoretical curves are acceptable estimates even in the later parts of the experiments. Comparisons for the other cases of table 1 lead to similar findings.

The open and crossed symbols corresponds to measurements of the density profiles in the forced and unforced rooms, respectively. Solid symbols represent the sum of these results and correspond to the buoyancy excess in the whole box. The buoyancy

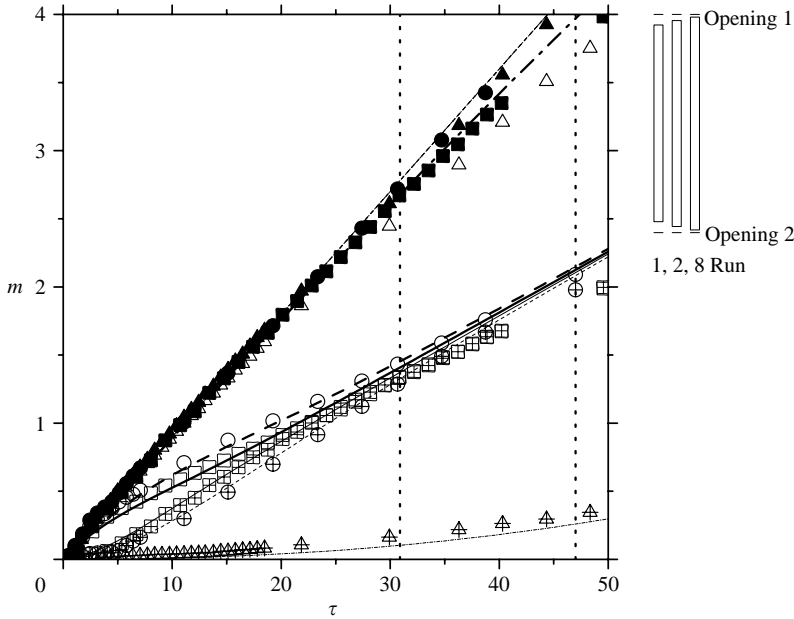


FIGURE 7. Experimental evolution of the buoyancy excess (symbols) when the opening size is varied as shown at the top right-hand side. The theoretical predictions are indicated by a solid line for Run 1, a dashed line for Run 2 and a dash-dotted line for Run 8. The times  $t_s$  at which mixed fluid is seen to flow out through the exit holes in Runs 1 and 2 are marked with vertical dotted lines. ( $R = 1$ ;  $\xi_1 = 1$ ;  $\xi_2 = 0$ .)

excess in the forced room is always greater than that in the unforced room even though they converge with time. Therefore, a buoyancy difference drives a flow from the forced to the unforced room through opening 1 as observed in the experiments. Consistently, a flow from the unforced room to the forced room through opening 2 is established, as shown in figures 2 and 4.

Figure 7 confirms that the reduction of the opening size increases the average density difference between the rooms with a reduction of the flow between them, as discussed in § 2.4. Also a reduction of the opening size is then accompanied by an increase of  $t_s$ , suggesting a reduction of the overall mixing (the time  $t_s$  for the smallest opening case falls outside the range of the abscissa).

### 3.3. Effects due to the change of the opening 1 height

Figure 8 shows the density profiles measured at different times when  $\xi_2 = 0$  and the opening 1 of equal size is located at different positions on the internal wall in Runs 1, 5 and 6, as indicated at the top right-hand side.

Since the fluid input is the same for the three experiments, the total buoyancy inside the box at a given time is the same provided that mixed fluid was not drained through the exit holes. The density profile in the forced room evolves as in an isolated room until the density interface reaches opening 1. In fact, the forced room contains all the fluid introduced by the source in the case with the lowest  $\xi_1$  (Run 6 - dotted line) at  $\tau = 6.7$ . At this time, opening 1 located at an intermediate position (dashed line) allowed the passage of mixed fluid to the unforced room. The maximum density difference in the unforced room is less than that for the experiment with  $\xi_1 = 1$  (solid line). The density interface in the forced room is found to be sharper in this case.

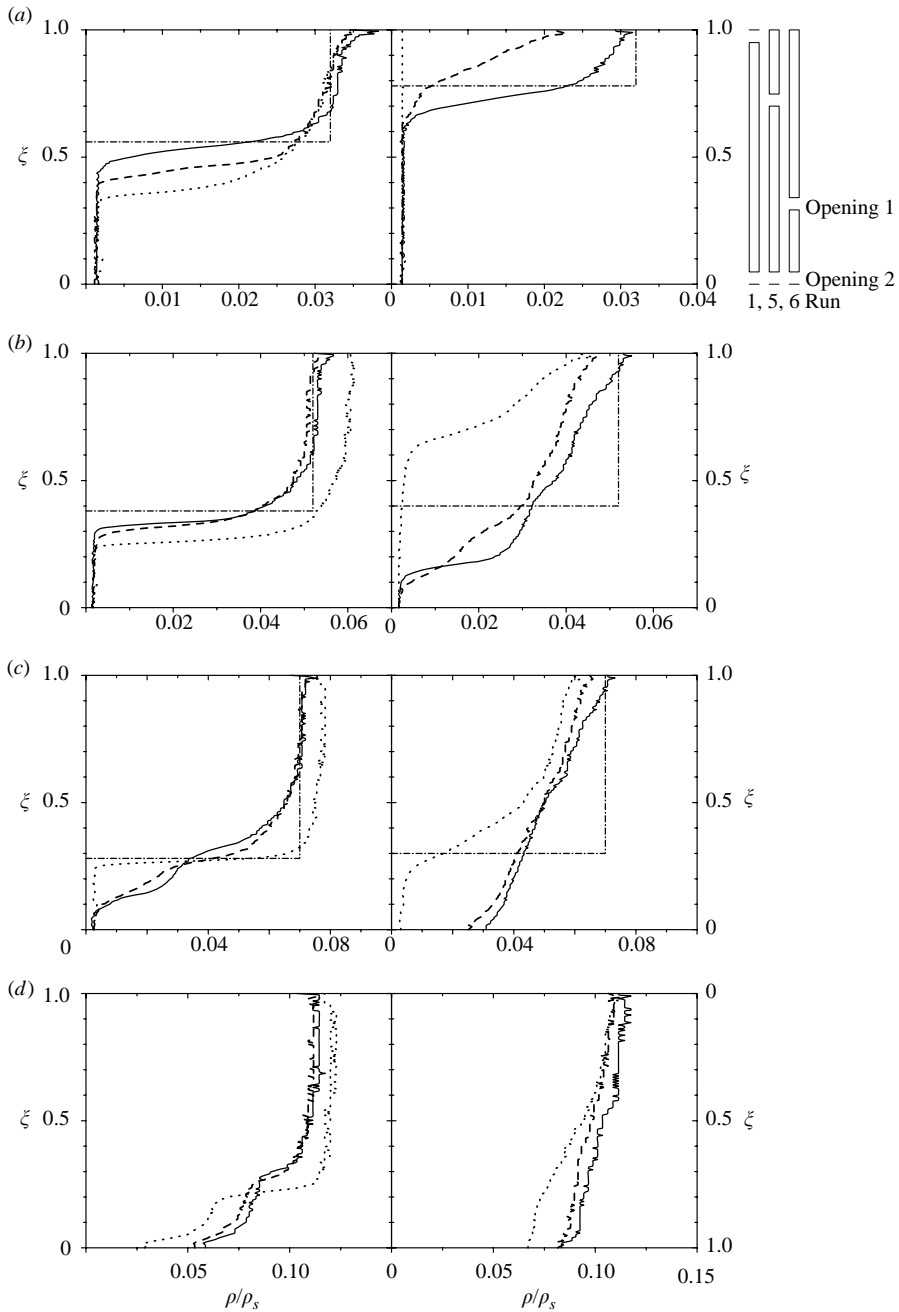


FIGURE 8. Density profiles in the forced (left) and unforced (right) rooms at times (a)  $\tau = 6.7$ , (b) 21, (c) 35, (d) 82. Opening 2 is at the bottom in the three experiments and opening 1 at different positions on the shared wall as shown at the top right-hand side. The solid, dashed and dotted lines correspond to Runs 1, 5 and 6, respectively. The equivalent profiles given by the model for Run 1 are also included in the graphs (box-shaped dash-dotted lines).

The equivalent profiles for Run 1 given by the theoretical model are included in figure 8(a-c). The uniform density layers adopted by the model give a rough approximation of the real density profile. However, the experimental buoyancy values

calculated by integration of the density profiles, and therefore the flow between the rooms, differ only about 5% from the model results.

At  $\tau \geq 21$ , the profiles for the experiment with  $\xi_1 = 1$  (Run 1) and with an intermediate position of opening 1 (Run 5) become similar in both chambers. On the contrary, opening 1 located at the lower position (Run 6), allowed the passage of only a small volume of dense fluid to the unforced room. The density profile is smooth there, while a higher density interface than that of the other two cases is observed in the forced room. Later (figure 8c), this interface becomes sharper, but its rate of rise decreases as a consequence of the flow of the dense fluid to the unforced room. This stronger flow rate to the unforced room increases the buoyancy excess faster there, tending to the values of the other cases, and the interface reaches the top of the unforced room after  $\tau = 35$ . Finally, for later times, all the profiles tend to be similar (figure 8d).

The buoyancy excess as a function of the dimensionless time  $\tau$  is seen in figure 9. The curves and the values of  $t_s$  are similar for the two runs with opening 1 at the highest positions. In contrast, in Run 6 the buoyancy excess evolves in a quite different way. The time  $t_s$  is almost twice the value of the other cases, but also the buoyancy excess difference between the rooms is higher. For  $t/t_s > 1$ , the total buoyancy excess is observed to depart from the linear behaviour because mixed fluid is being released from the exit holes. Figure 9(b) shows the same results, but with time and buoyancy excess non-dimensionalized with  $t_s$  and the buoyancy excess  $m_s$  at that time, respectively. The different behaviour for  $t/t_s < 1$  in the three cases indicates that the height of the openings not only changes  $t_s$ , but also the mixing rate inside the box. The density difference between the rooms is maintained for a longer time than  $t_s$ .

In summary, a lower height of opening 1 maintains a higher buoyancy excess difference between the rooms, reduces the overall mixing and increases  $t_s$ .

#### 3.4. Effects of the change of opening 2 height

Density profiles obtained in the experiments with openings of equal size,  $\xi_1 = 1$  and opening 2 located at different positions on the shared wall are shown in figure 10. The stratification in both chambers is strong and the profiles are similar at  $\tau = 6.7$ , suggesting that the position of the lower opening has not yet influenced the flow inside the box. A difference appears when the interface in the unforced room reaches the lower opening (figure 10b). In such a situation, the interface in the unforced room starts to move downwards with a velocity imposed by the mass flux from the nozzle, which pushes ambient fluid through the exit holes. Meanwhile, the density in the forced room increases steadily, and so the density of the fluid passing to the unforced room increases giving a non-uniform density profile. The interface and the fluid trapped in the lower part of the unforced room move downward and eventually reach the floor (figure 10c). Finally, the mixed fluid starts to leave the box and the profiles tend to be uniform for later times (figure 10d).

The buoyancy excess evolves consistently with the previous results. It is found that for higher  $\xi_2$  the time for which the mixed fluid begins to leave the box is longer, and the buoyancy excess difference between the rooms is maintained for a longer time than  $t_s$ .

#### 3.5. Different heights of both openings

Figure 11 shows a comparison of the evolution of the buoyancy excess among four cases in which opening 1 does not fall below, and opening 2 does not exceed, half the total height. For  $\tau \lesssim 20$  (see inset of figure 11), the evolution of  $m$  in Run 1 is

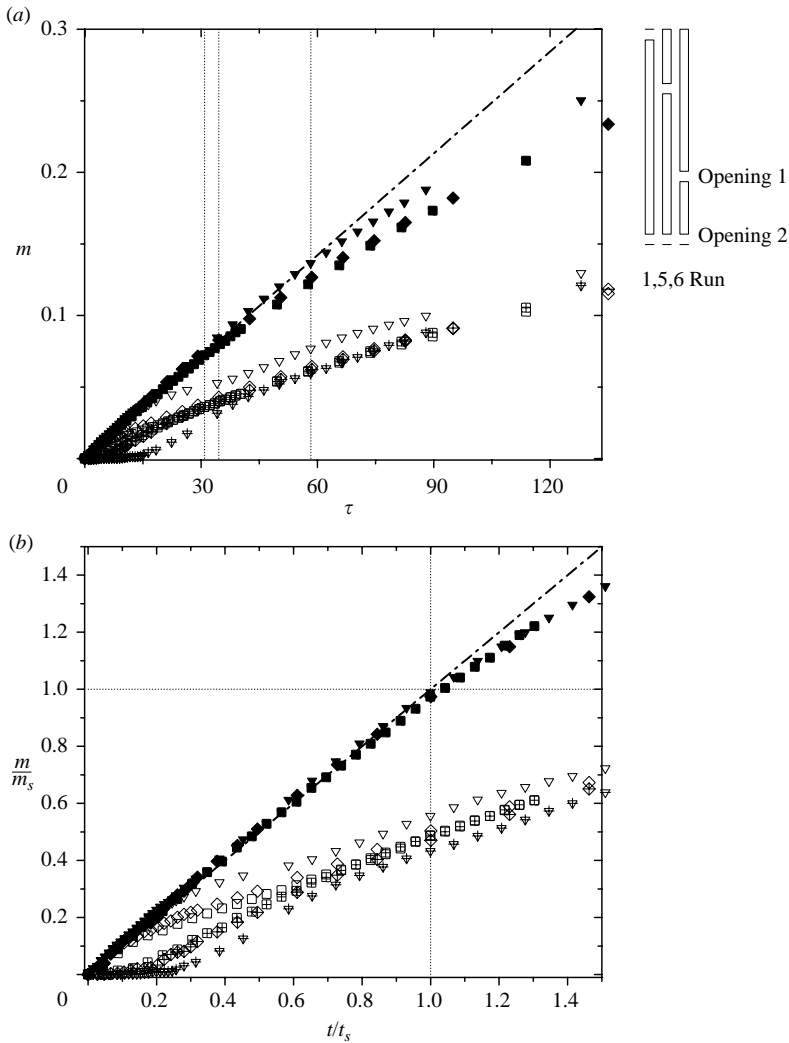


FIGURE 9. (a) Evolution of the buoyancy excess contained in the forced room (open symbols), in the unforced room (crossed symbols) and in both rooms (solid symbols) for the experiments of figure 8. (b) Evolution of the buoyancy excess non-dimensionalized with the values of  $m_s$  and  $t_s$  corresponding to each experiment. Symbols correspond to Runs 1 (squares), 5 (diamonds) and 6 (down triangles).

close to that in Run 3 because opening 1 is at the top of the shared wall causing the flow to the unforced room to be established immediately after the plume reaches the top of the forced room in both cases. For  $\tau \gtrsim 100$  (figure 11), the progress of  $m$  in Run 1 tends to be similar to that in Run 5 once opening 1 is reached by the interface in the forced chamber; time  $t_s$  is found to be nearly the same for these runs. The same happens for experiments 3 and 7, even though the corresponding times  $t_s$  are somewhat different. The similitude of the evolution is maintained for long times (i.e. for  $t \gg t_s$ ) indicating that the rate of mixed fluid leaving the box through the exit holes, and therefore mixing inside the box, are mainly affected by the position of opening 2.

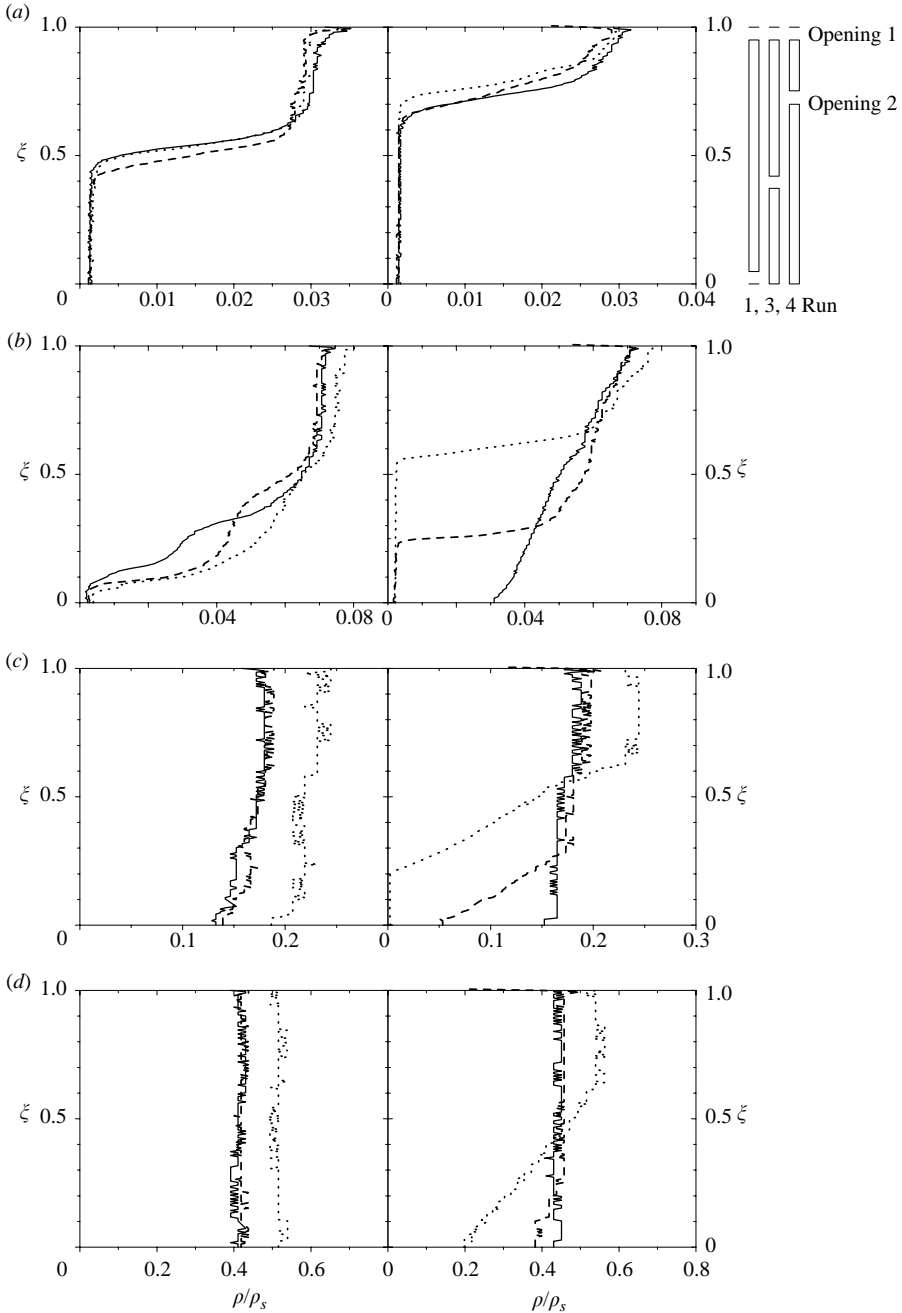


FIGURE 10. Density profiles in the forced (left) and unforced (right) rooms at times (a)  $\tau = 6.7$ , (b) 35, (c) 167, (d) 387. One opening is located at the top and the other, of equal size, at different positions on the shared wall, as shown at the top right-hand side. The solid, dashed and dotted lines correspond to Runs 1, 3 and 4, respectively.

#### 4. Conclusions

We have studied analytically and experimentally the flow driven by density differences between two interconnected rooms generated by a single heat source. In particular, we have analysed the features of the transient convective flow for



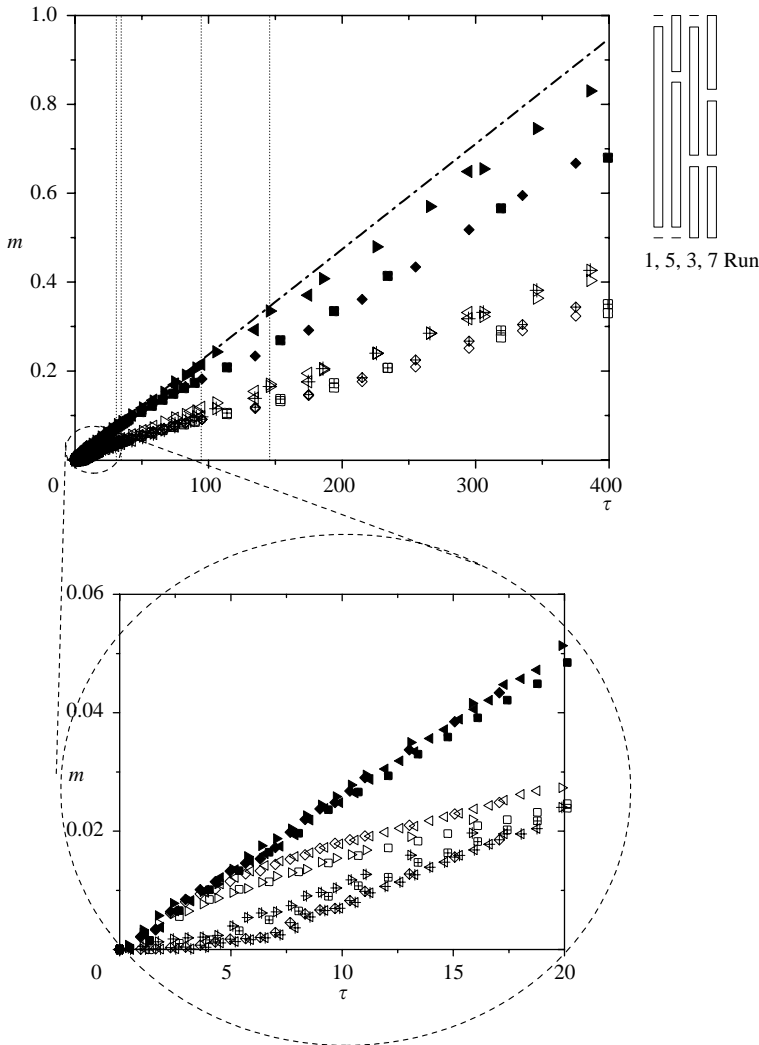


FIGURE 11. Evolution of the buoyancy excess contained in the forced room (open symbols), in the unforced room (crossed symbols) and in both rooms (solid symbols) for Runs 1 (squares), 5 (diamonds), 3 (right-hand triangles) and 7 (left-hand triangles) for  $0 < \tau < 400$ . Vertical dotted lines indicate the time  $t_s$ . The inset shows an enlargement of the same results for  $0 < \tau < 20$ .

different positions and sizes of the two openings located on the vertical wall shared by the rooms.

The evolution of the stratification in the rooms is described by an analytical model that estimates the flow using the hydrostatic pressure on both sides of the openings by simplifying the density profiles inside the warm layers. The model provides good quantitative results from the time when the heat source is turned on, up to the time  $t_s$  when the interface in the unforced room reaches the ceiling. After the time  $t_s$ , the theoretical prediction departs gradually from the experimental results because the total buoyancy excess is not maintained in the experiments, but it may be considered as a reasonable estimate according to the findings of § 3.2.

The theoretical model introduced here improves and generalizes previous models and allows the analysis of situations in which the openings are located at different

Effect	Consequences					
	Overall mixing	Average density difference		$t_s$	$t_s$ (s)	Run
		between rooms				
Openings at the top & bottom		Taken as reference			460	1
Reduction of opening size	Reduction	Increase	Increase	705, 6800	2, 8	
Lower opening 1	Reduction	Increase	Increase	520, 870	5, 6	
Higher opening 2	Reduction	Increase	Increase	2190, 3780	3, 4	
Lower opening 1 + higher opening 2	Reduction	Increase	Increase	1420	7	

TABLE 2. Results obtained arranged by effect.

heights on the shared wall. Thus the height  $\xi_{ss}$  for the steady-state ventilation of a single room as a function of  $\xi_1$  is obtained as illustrated in figure 3. Buoyancy conservation for determining the advance of the fronts is used instead of volume conservation employed previously, obtaining better predictions. The heights of the interfaces may be higher or lower than the neutral level, a situation that allows us to study more complex configurations and regimes. In addition, the concept of an equivalent layer of a non-uniform density profile, as proposed by Marino *et al.* (2005), is included in the theoretical approach to improve the physical understanding but also to simplify the mathematical equations giving an analytical solution of the problem.

The condition (2.30) determines the importance of the opening size on the flow. Stratification in the forced room evolves as in a closed room if  $A^*/H^2 \ll (C/\theta)^{3/2} \approx 0.03$ ; the forced room is strongly ventilated to the unforced room in the opposite situation and then the aspect ratio  $R$  may affect the evolution of the flow in both rooms.

At the beginning, the flow is determined mainly by the position of the opening furthest from the source (opening 1). If this is at the top on the shared wall, the flow to the unforced room is established just after dense fluid reaches the ceiling of the forced room. The position of opening 2 determines the volume of the unforced room that does not participate in the flow. In fact, all the fluid of the unforced room below opening 2 remains with the initial density.

The experiments provide useful insights into the mixing and the effects produced by the volume flux from the source. The flow develops similarly up to about 15–20 characteristic times in all cases, confirming that the characteristic time  $t_f = S_f B^{-1/3} H^{-2/3}$ , introduced in §2, is supported by the experimental results even in the presence of mixing.

The results of the experiments, which are summarized in table 2, show that a reduction in the size of the opening, the reduction in height of opening 1 or the elevation of opening 2, increases  $t_s$  and alters the efficiency of the heating system. An increase of  $t_s$  means a decrease of the overall mixing accompanied by an increase of the density difference between the rooms. However, these consequences are nonlinear with the magnitude of the effect or with its combination, and further study of the flow including the mixing is required.

This work was supported by CONICET (Argentina) under Grants PIP 2826 and 5893, CONACYT (Mexico) project U41347-F and by a grant from the UC MEXUS-CONACYT.

## REFERENCES

- ALI, S. K. & FOSS, J. F. 2003 The Discharge coefficient of a planar submerged slit-jet. *Trans. ASME I: J. Fluids Engng*, **125**, 613–619.
- BAINES, W. D. & TURNER, J. S. 1969 Turbulent buoyant convection from a source in a connected region. *J. Fluid Mech.* **37**, 51–80.
- CENEDESE, C. & DALZIEL, S. B. 1998 Concentration and depth field determined by the light transmitted through a dyed solution. In *Proc. 8th Intl Symp. on Flow Visualization* (ed. G. M. Carlo-Magno & I. Grant). ISBN 0953399109, paper 061 (CD rom).
- DALZIEL, S. B. 1993 Rayleigh–Taylor instability: experiments with image analysis. *Dyn. Atmos Oceans* **20**, 127–153.
- DALZIEL, S. B. 1995 *DigImage: System Overview*. Cambridge Environmental Research Consultants, UK.
- HUNT, G. R. & KAYE, N. G. 2001 Virtual origin correction for lazy turbulent plumes. *J. Fluid Mech.*, **435** 377–396.
- LIN, Y. J. P. & LINDEN, P. F. 2002 Buoyancy-driven ventilation between two chambers. *J. Fluid Mech.* **463**, 293–312.
- LINDEN, P. F. 1999 The fluid mechanics of natural ventilation. *Annu. Rev. Fluid Mech.* **31**, 201–238.
- LINDEN, P. F., LANE-SERFF, G. F. & SMEED, D. A. 1990 Emptying filling boxes: the fluid mechanics of natural ventilation. *J. Fluid Mech.*, **212**, 300–335.
- MARINO, M. B., THOMAS, L. P. & LINDEN, P. F. 2005 The front condition for gravity currents. *J. Fluid Mech.* **536**, 49–78.
- MORTON, B. R., TAYLOR, G. I. & TURNER, J. S. 1956 Turbulent gravitational convection from maintained and instantaneous sources. *Proc. R. Soc. Lond. A* **234**, 1–23.
- TURNER, J. S. 1986 Turbulent entrainment: the development of the entrainment assumption. *J. Fluid Mech.* **173**, 431–472.
- WORSTER, M. G. & HUPPERT, H. E. 1983 Time-dependent density profiles in a filling box. *J. Fluid Mech.* **132**, 457–466.